CHEMISTRY
AN ASIAN JOURNAL
www.chemasianj.org

Title: Syntheses and properties of meso-substituted porphyrin mesogens with triazole linkages and peripheral alkyl chains

Authors: Ruilin Zhang, Hongfei Gao, Yanming Ren, Yulong Xiao, Jinliang Hu, and Xiaohong Cheng

To be cited as: *Chem. Asian J.* 10.1002/asia.201701666

Link to VoR: http://dx.doi.org/10.1002/asia.201701666

A Journal of
ACES
Asian Chemical Editorial Society

A sister journal of **Angewandte Chemie** and **Chemistry – A European Journal**

WILEY-VCH

10.1002/asia.201701666

Syntheses and properties of *meso*-substituted porphyrin mesogens with triazole linkages and peripheral alkyl chains

Ruilin Zhang,[a,b]‡ Hongfei Gao,[a]‡ Yanming Ren,[a] Yulong Xiao,[a] Jinliang Hu,[a] Xiaohong Cheng*[a]

[a] Key Laboratory of Medicinal Chemistry for Natural Resources, Ministry of Education, Chemistry School of Chemical Science and Technology, Yunnan University, Kunming, Yunnan 650091, P. R. China
Fax: (+86) 871 65032905
E-mail: xhcheng@ynu.edu.cn

[b] Forensic Medicine of Kunming Medical University, Kunming, Yunnan 650500, P. R. China

‡ Both authors contributed equally to this work.

Abstract: Novel discotic mesogens **P/*n*-M** (*n* = 12, 16, 18, M = 2H, Zn and Cu) bearing a porphyrin core, triazole linkages and peripheral 3,4,5-trialkoxybenzyl units have been synthesized by “click chemistry” approach. The thermal behavior, photophysical properties and morphologies of these compounds were investigated by polarizing optical microscopy (POM), differential scanning calorimetry (DSC), X-ray diffraction (XRD), UV and PL spectra, scanning electron microscopy (SEM) and transmission electron microscopy (TEM). These compounds can self-assemble into hexagonal columnar phases in their pure states and form organogels in 1,4-dioxane with unusually flower-like sphere morphology. The supramolecular complexes of **P/18-Zn** with C_{70} or 4,7-di-4-pydriyl-2,1,3-benzothadiazole can display hexagonal columnar phases too. Additionally, zinc porphyrin compounds **P/*n*-Zn** show binding selectivity to Cu^{2+} among a series of cations in THF-H_2O solution.

1 Introduction

Porphyrin is a large heteroaromatic planar molecule which consists of four conjugated pyrrole subunits connected through methylene linkages. The porphyrins are interesting because their physical and chemical properties can be tuned either by the substitute in the periphery or by the central metal ion. Porphyrins are used as cores in the syntheses of columnar liquid crystals (LCs) [1]. Columnar phases are important because of their one-dimensional (1D) aromatic π-π stacking [2] leading to one-dimensional charge conduction [3], which may improve the charge-carrier mobility. One of the advantages of mesomorphic porphyrins over many other discotic macrocycles is their strong absorption in the visible and NIR regions. Porphyrin occurs in nature (chlorophyll), and rothemund is the firstly synthesized porphyrin [4]. The uro-porphyrin(I)octa-*n*-dodecyl ester is the first porphyrin based mesogen reported by Goodby et al [5]. Later *meso*-substituted porphyrin meogens (Fig. 1) with amide [6,7,8] or ester linkages [9,10,11,12] and peripheral alkyl or semiperfluoroalkyl chains [13] were reported. These mesogens displayed usually rectangular and hexagonal columnar mesophases. Unsymmetrical β-polysubstituted porphyrin (Fig. 2) synthesized from natural porphyrin hemin showing ordered hexagonal columnar phases (Col$_{ho}$), hexagonal columnar phases (Col$_{h}$) as well as discotic lamellar mesophase were reported too [14,15,16]. Some of the columnar phases can be homeotropically aligned in their pure state [10,12,13] or in the mixture with 1-(3-methoxycarbonyl)propyl-1-phenyl-(6,6)C$_{61}$ (PCBM) [17], which holds great promise for high-performance electronic devices. Ferroelectric coordination polymers are also realized by the co-assembly of lipophilic zinc porphyrin (ZnP) with ditopic bridging ligands [18].

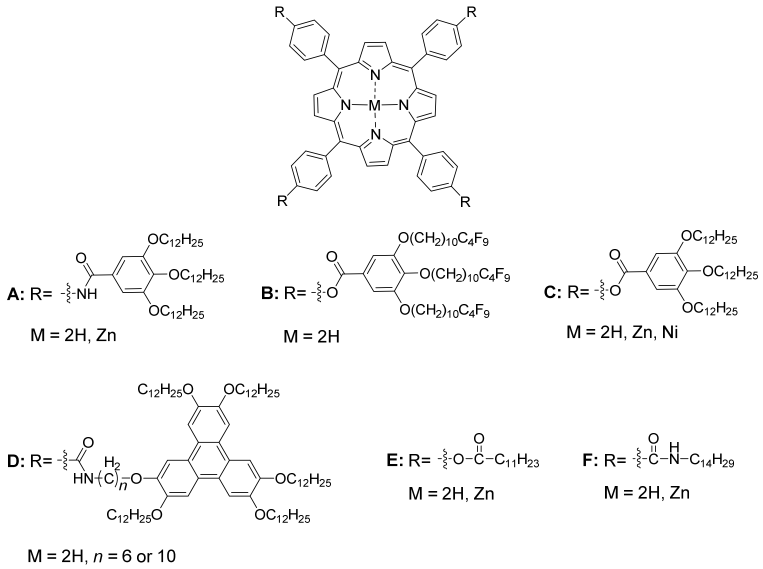

Fig. 1 The reported *meso*-substituted porphyrin mesogens [6,7,8,9,10,11,12,13].

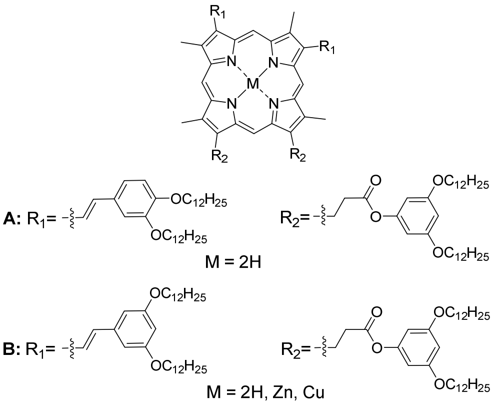

Fig. 2 The reported β-polysubstituted porphyrin mesogens [14,15,16].

Copper-catalyzed azide–alkyne (CuAAC) click reaction affords 1,2,3-triazoles as a chemical links in construction of a variety of conjugated molecules. Via click chemistry, porphyrins have been connected with various scaffolds such as fullerene [19,20,21], ferrocene [22] and carbohydrate [23] in a single molecular framework for the study of their photophysical and therapeutic properties. In addition, 1,2,3-triazole subunit is also found useful in the synthesis of *meso*-*meso* linked porphyrin dimers [24] and carbon nanotube functionalized porphyrin analogues [25]. The application of a 1,2,3-triazole ring in coordination with metal ions [26] and as hydrogen bonding acceptor or donor to construct of supramolecules [27] are also reported. However to our surprise, till now there is no porphyrin mesogens containing the 1,2,3-triazole linkages been reported.

Therefore herein *meso*-substituted porphyrins (Scheme 1) with triazole linkages and peripheral alkyl chains **P/*n*-2H** and their metal coordination compounds **P/*n*-Zn** and **P/*n*-Cu** were synthesized efficiently by the click reaction. The self-assembly behaviors, photophysical properties, and chemosensor behaviors of these compounds have been studied.

2 Results and discussion

2.1 Synthesis

The metal free porphyrin target compounds **P/*n*-2H** were synthesized by the CuAAC click reaction between porphyrin tetaracetylene **2** and benzyl azide **3/*n*** (Scheme 1) [28]. The porphyrin tetaracetylene **2** was synthesized through the reaction between 4-(prop-2-yn-1-yloxy)benzaldehyde **1** and pyrrole in the presence of propionic acid [29]. The metal porphyrin complexes **P/*n*-Zn** or **P/*n*-Cu** were obtained from metal free porphyrin **P/*n*-2H** and zinc/copper acetate. All of the target compounds were purified by column chromatography. The detailed procedures and corresponding analysis data are collected in the Supporting Information (SI).

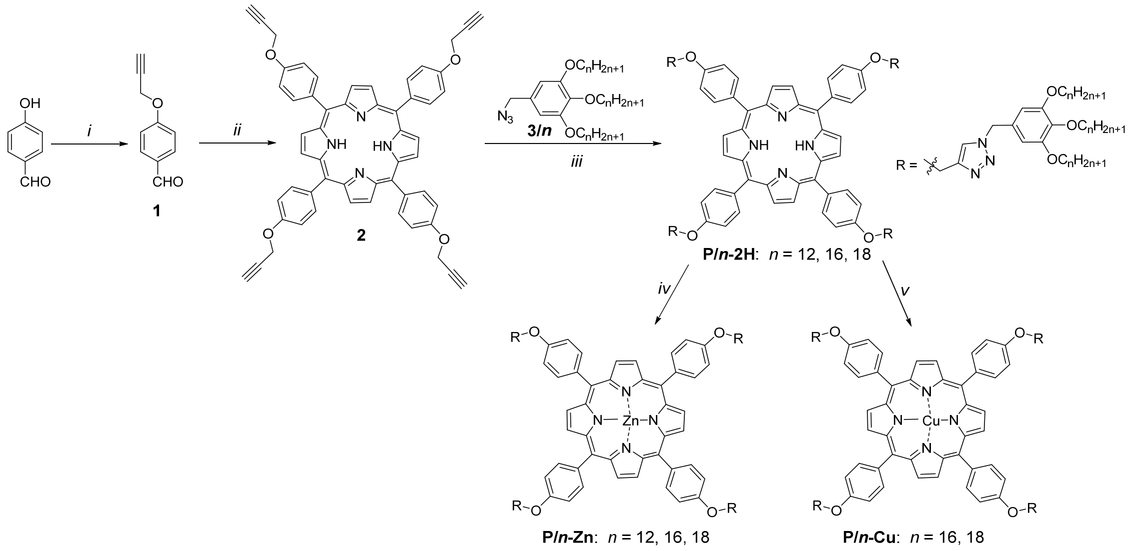

Scheme 1 Synthesis route for porphyrin derivatives **P/*n*-2H, P/*n*-Zn and P/*n*-Cu**. *Reagents and conditions*: (*i*) K_2CO_3, propargyl bromide, acetone, 50 °C, 12 h, 88%; (*ii*) $EtCO_2H$, pyrrole, 120 °C, 1 h, 23%; (*iii*) $CuSO_4 \cdot 5H_2O$, sodium ascorbate, TBA : H_2O = 1 : 1, THF, 12 h, 65-78%; (*iv*) $Zn(Ac)_2 \cdot 2H_2O$, chloroform/methanol = 3 : 1, reflux, 24 h, 80-85%; (*v*) $Cu(Ac)_2 \cdot H_2O$, chloroform : methanol = 3 : 1, reflux, 24 h, 86-90%.

2.2 Mesomorphic behavior

The mesomorphic behaviors of these porphyrin compounds were investigated by POM, DSC and XRD. The phase transition temperatures and associated enthalpy values of these compounds are collected in Table 1. Compounds **P/12-2H** and **P/12-Zn** are crystals, all the other compounds **P/*n*-2H**, **P/*n*-Zn** and **P/*n*-Cu** with *n* = 16 and 18 are enantiotropic (thermodynamically stable) LCs. By coordination with metal ions, the decreasing of melting temperature and the increasing of the clearing temperature were observed, therefore these metal coordination compounds **P/*n*-Zn** and **P/*n*-Cu** show wider mesophase temperature ranges than their corresponding metal free parent compounds **P/*n*-2H**. It is reasonable to deduce that the metalation of porphyrin cores leads to the increase of both the rigidity and their electrostatic attraction of the porphyrin rings [30]. Furthermore, the Zn coordination compounds **P/*n*-Zn** have wider mesophase temperature ranges than their corresponding Cu coordination compounds **P/*n*-Cu** (Fig. S1).

Table 1 The phase transition temperatures, associated enthalpy values (in brackets), lattice parameters and molecular dimensions of compounds **P/*n*-2H**, **P/*n*-Zn**, **P/*n*-Cu**^{a}

Comp.	T/°C [ΔH/kJ mol^{-1}]	a[nm] (T/°C)	L [nm]	Z
P/12-2H	Cr$_1$ 46.8 [9.6] Cr$_2$ 143.7 [52.6] Iso	-	-	-
P/12-Zn	Cr 101.3 [3.0] Iso	-	-	-
P/16-2H	Cr 36.0 [142.2] Col$_{hex}$ 110.8 [6.7] Iso	4.71 (100)	8.2	1.2
P/16-Zn	Cr 20.6 [80.9] Col$_{hex}$ 118.1 [3.8] Iso	4.64 (110)	8.2	1.2
P/16-Cu	Cr 26.0^b Col$_{hex}$112.0^b Iso	4.64 (110)	8.2	1.2
P/18-2H	Cr 56.8 [151.2] Col$_{hex}$ 103.7 [2.6] Iso	4.96 (95)	8.6	1.3
P/18-Zn	Cr 43.4 [153.9] Col$_{hex}$ 122.2 [3.8] Iso	4.86 (90)	8.6	1.2
P/18-Cu	Cr 52.2 [122.9] Col$_{hex}$ 117.0 [3.4] Iso	4.95 (100)	8.6	1.2

^{a}Transition temperatures were determined by DSC (5 K min^{-1}) and confirmed by POM, peak temperatures from the second heating scan are given. Abbreviations: Cr = crystal; Col$_{hex}$ = hexagonal columnar phase; Iso = isotropic liquid; a = lattice parameter; L = maximum molecular length in the most extended conformation; Z = number of molecules in the cross section of a column in the Col$_{hex}$ phases (with assumed height of 0.45 nm). ^{b}Transition temperature was determined by POM.

Between crossed polarizers, the textures of all the LC phases show birefringent and in most cases spherulitic textures, as typical textures of columnar mesophase (see Fig. 3a and Fig. S2a-e) [31]. All these columnar phases are uniaxial, as indicated by the presence of optically isotropic homeotropic regions, where the direction of the cylinder long axis is perpendicular to the substrate surfaces (the dark areas in Fig. 3a and Fig. S2a-e). This means that the investigated columnar phases could either have a hexagonal or a square 2D lattice.

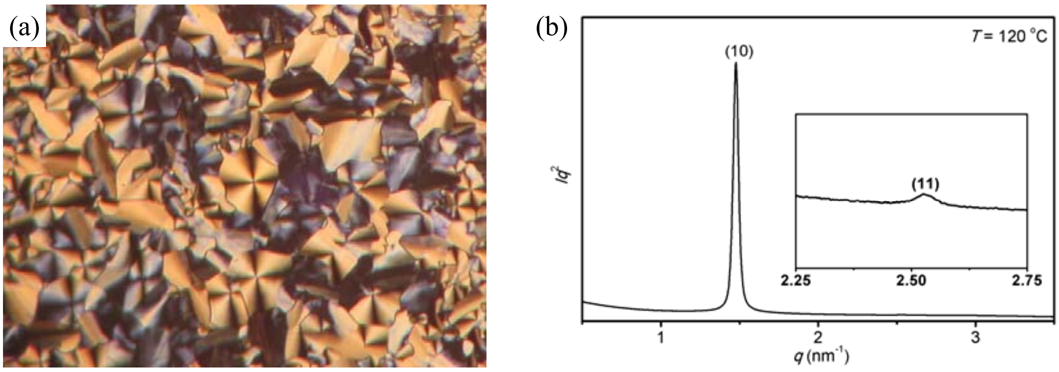

Fig. 3 (a) Polarizing optical textures of **P/18-Cu** at T = 93 °C; (b) SAXS diffractogram of Col$_{hex}$ phase at T = 120 °C.

These LC phases were also investigated by small-angle X-ray scatting (SAXS). There are two or three diffracting peaks in the small angle region with a ratio of reciprocal spacings of 1 : 3$^{1/2}$ (: 2). The diffraction peaks of the SAXS could be indexed to the 10, 11, (and 20) reflections of a hexagonal lattice (Fig. 3b and Fig. S4a-e and Table S1-S6). The lattice parameters are summarized in Table 1. Based on these lattice parameters, the number of molecules Z organized in a stratum of the columns with a height of h = 0.45 nm was estimated by using Equation (1) and assuming a density of ρ = 1 g·cm^{-3} (N_A = Avogadro constant, M = molecular mass) to be about 1 (see Table 1).

$$Z = (a^2/2)\sqrt{3}(N_A/M)\rho \qquad (1)$$

The molecules should self-assemble into 1D columns eventually leading to 2D hexagonal columnar mesophases [32]. In these columnar phases, the stacking of the molecules should be driven by the microsegregation of the polar central moieties from the alkyl chains and simultaneously the dense packing of the core units. It should be noted that the intercolumnar distance (namely the lattice parameter) of these hexagonal columnar phases is much smaller than the fully extended molecular length of porphyrin derivatives (calculated by MM2 method [33], see Table 1), indicating strong interdigitation and folding of the lipophilic alkyl chains between the adjacent columns. The self-assembly model of hexagonal columnar phase is shown in Fig. 4c. This model is supported by the electron density map which was reconstructed from the SAXS intensities of compound **P/18-Cu** (Fig. 4a). The purple and blue areas in the middle of the columns represent the regions with the highest electron density, which can be assigned to the column centers formed predominately by the porphyrin rings. The green medium electron density shells are formed by the benzyl, triazole and phenyl groups while the red areas (lowest electron density) should represent the continuum of the fluid alkyl chains. The molecular dynamics (MD) annealed model [34] of the columnar phase shows that the porphyrin rings form the columnar cores and the benzyl, triazole and phenyl units form a kind of shell separating the porphyrin core from the aliphatic continuum, in which the alkyl chains are completely disordered and strongly interdigitated (Fig. 4b). This model is in well agreement with the reconstructed electron density maps of the Col$_{hex}$ phase [35].

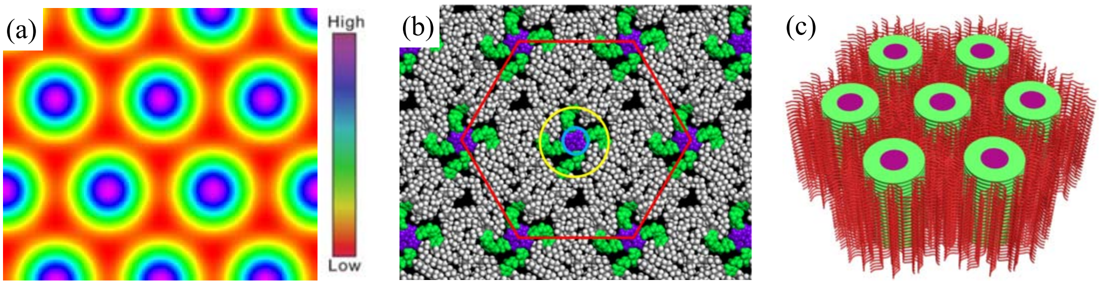

Fig. 4 (a) Reconstructed electron density map of the Col$_{hex}$ phase of **P/18-Cu**; (b) Snapshot of the structure of the Col$_{hex}$ phase of **P/18-Cu** after MD annealing (porphyrin cores are colored purple and the benzyl, triazole and phenyl groups are colored green, alkyl chains gray); light blue and yellow circles represent the boundaries between high and medium and medium and low electron density regions in the electron density maps, respectively; (c) The model for Col$_{hex}$ phase.

2.3 Photoelectric properties

The UV-vis absorption spectra of the CH_2Cl_2 solutions, the thin films, as well as the gels of the representative compounds **P/18-2H**, **P/18-Zn** and **P/18-Cu** are shown in Fig. 5a and Fig. S6, and the corresponding spectral data are collected in Table 2. In the CH_2Cl_2 solutions, these compounds display strong Soret bands at around 420 nm and weak Q bands from 500 to 650 nm as typical of porphyrin absorption [36]. The Soret and Q bands in the compound **P/18-Zn** are found to be red-shifted by 4-11 nm as compared to free porphyrin **P/18-2H**. In contrast, the Soret and Q bands in **P/18-Cu** are found to be little blue-shifted by 1-2 nm as compared to free porphyrin **P/18-2H** [37]. The red shifts of the Soret bands of the films were more pronounced than in solution because of greater aggregation and planarity of the molecules leading to higher conjugation in films (Fig. S6a). In addition, Fig. S6b showed that the Soret bands of the target compounds in gel phases shifted to longer wavelengths comparing to that of the target compounds in CH_2Cl_2 solution. This indicated that the target molecules assemble into a *J*-aggregate in the gel phase [38]. The optical energy band gaps (E_g^{opt}) of compounds **P/18-2H**, **P/18-Zn** and **P/18-Cu**, which were estimated from the onsets of the absorption in thin films, are 2.12 eV, 1.93 eV and 2.15 eV respectively (Table 2 and Fig. S7) [39]. The HOMO and LUMO energy levels of **P/18-2H**, **P/18-Zn** and **P/18-Cu** in thin films were determined by cyclic voltammetry on a glassy carbon electrode (Fig. S8 and Table S9) from the onsets of oxidative and reductive potentials. The band gaps were almost in agreement with those obtained from their absorption spectra in thin films. These absorption data are favorable for light-harvesting and are expected to afford better cell performance.

The fluorescence emission spectra of compounds **P/18-2H**, **P/18-Zn** and **P/18-Cu** in CH_2Cl_2 solutions are shown in Fig. 5b. Compound **P/18-Zn** displays a structured emission with maxima at 604 nm and 652 nm. In contrast, the compound **P/18-2H** has shown very poor emission, no emission was observed in the case of copper derivative **P/18-Cu** under the same experimental conditions due to the paramagnetic nature of copper (II) ion [40].

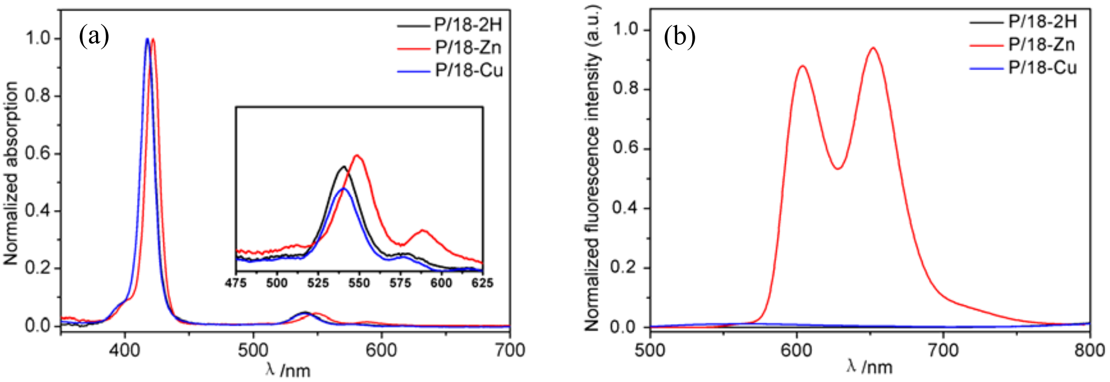

Fig. 5 UV-vis absorption spectra (a) and fluorescence emission spectra (b) of compounds **P/18-2H**, **P/18-Zn** and **P/18-Cu** in CH_2Cl_2 (5.0×10^{-6} M) (excited at 418 nm, 422 nm and 417 nm, respectively).

Table 2 UV-vis absorption spectral maxima of the compounds **P/18-2H**, **P/18-Zn** and **P/18-Cu**

Comp.	Soret band/nm			Q bands/nm		Q bands/nm		E_g^{opt}/eV
	CH_2Cl_2	film	gel	CH_2Cl_2		film		
P/18-2H	418	422	423	541	577	547	-	2.12
P/18-Zn	422	439	435	549	588	566	608	1.93
P/18-Cu	417	419	420	540	575	546	585	2.15

2.4 Chemosensor behavior

Compound **P/18-Zn** was selected for metal ion recognition. This was examined by monitoring the change of fluorescence intensity upon the addition of 10 equiv. solutions of various metal ions, including Zn^{2+}, Ni^{2+}, Ag^{+}, Cd^{2+}, K^{+}, Mg^{2+}, Cu^{2+}, Co^{2+}, Li^{+}, Pd^{2+}, Hg^{2+} and Fe^{3+}. As can be seen in Fig. 6, the fluorescence emission was significantly quenched by Cu^{2+}.

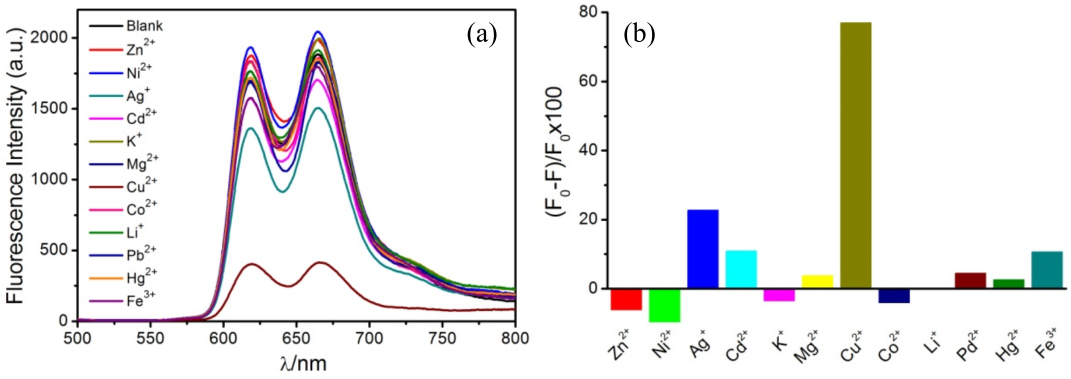

Fig. 6 (a) Fluorescence spectra at room temperature at pH = 7.0 in THF : H_2O = 1 : 1 mixture (λ_{ex} = 422 nm) of **P/18-Zn** (5.0×10^{-6} M); (b) $(F_0\text{-}F)/F_0 \times 100$ depicts the cation selective fluorescence quenching efficiency namely the fluorescence responses of different metal ions of **P/18-Zn**; abbreviation: F_0 = the fluorescence emission maximum of the blank sample; F = the fluorescence emission maximum of samples after addition of different metal ions.

For the selective response of **P/18-Zn** to Cu^{2+}, fluorescence titration was performed in THF : H_2O = 1 : 1 solution. With the addition of Cu^{2+} (from 1 to 20 equiv.), the emission peak at 618 nm and 664 nm decreased gradually and finally reached its fluorescence quenching plateau at ~ 15 equiv. (Fig. 7) [41]. In order to investigate the binding site of **P/18-Zn** with Cu^{2+}, FTIR spectra of **P/18-Zn** and **P/18-Zn+Cu^{2+}** were performed (Fig. S9). The spectrum in Fig. S9 indicated that the N=N stretching vibrations of triazole ring of **P/18-Zn** are located at 1658 cm^{-1} [42]. After adding 10 equiv. Cu^{2+}, N=N of triazole ring shows blue shift from 1658 cm^{-1} to 1643 cm^{-1}, indicating that the binding site of **P/18-Zn** to Cu^{2+} is much likely to coordinate to the N atom of triazole ring. However, we were unable to probe further the binding mechanism between **P/18-Zn** and Cu^{2+} by NMR due to the paramagnetic nature of Cu^{2+} [43]. The paramagnetic nature of Cu^{2+} ion with an unfilled *d* shell could strongly quench the fluorescence of **P/18-Zn** through the electron or energy transfer mechanism (Fig. S10) [44]. Therefore, compound **P/18-Zn** could be used as chemosensor exhibiting strong and selective binding to Cu^{2+} in THF : H_2O = 1 : 1 solution. Because Cu^{2+} is a significant environmental pollutant ascribed to its widespread application, the development of chemosensors for the detection and monitoring of Cu^{2+}, with high sensitivity, low detection limit and quick response, is in great demand [45].

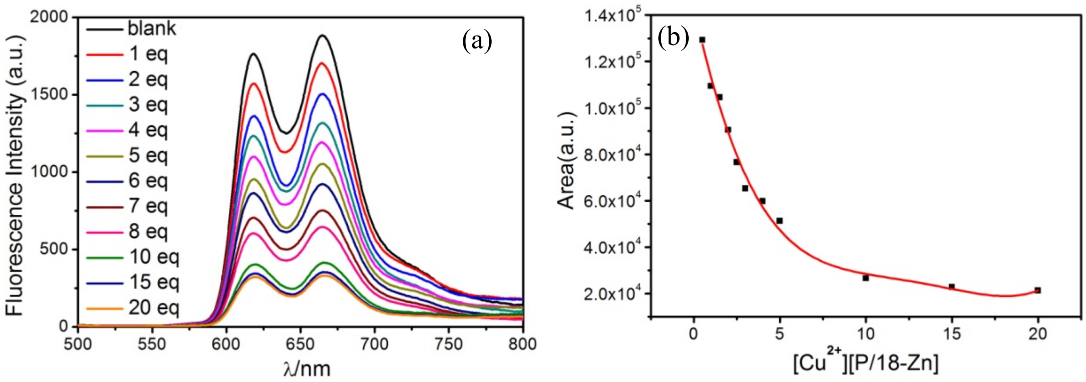

Fig. 7 (a) Fluorescence spectra of compound **P/18-Zn** (5.0×10^{-6} M) at room temperature upon addition of Cu^{2+} (from 0.5 to 20.0 equiv) in THF : H_2O = 1 : 1 (λ_{ex} = 422 nm); (b) The titration curve of the integrated fluorescence as a function of Cu^{2+} concentration.

2.5 Gel properties

The gel properties of the representative compounds **P/18-2H**, **P/18-Zn**, **P/18-Cu** are shown in Table 3. These compounds can form dark red gels in 1,4-dioxane. The metalation of porphyrin cores seems to have no influence on the gel properties of these compounds. These organogels exhibit a multiple reversible transition process upon exposure to a number of environmental stimuli including temperature and shear (Fig. 8). Such multiple stimuli-responsive properties may endow these gels with great potentials as drug controlled release [46], energy transfer [47], hardeners of solvents and sensors *etc.* [48]. To assess the gel stability, we measured T_{gel} (the temperature at which the gel is broken) values for the 1,4-dioxane gels of **P/18-2H**, **P/18-Z**n and **P/18-Cu** (Fig. S11). The T_{gel} values for **P/18-2H**, **P/18-Zn** and **P/18-Cu** increased with increasing gelator concentration, which is a general trend observed for low molecular weight gelators [49]. The T_{gel} values for **P/18-Zn** and **P/18-Cu** are somewhat higher than **P/18-2H**. The enhanced π-π interaction between neighboring porphyrins is believed to be responsible for this improvement, as metalation has been shown to increase both the rigidity of the porphyrin rings and their electrostatic attraction [30]. The morphologies of these organogels were investigated by scanning electron microscopy (SEM) and transmission electron microscopy (TEM). Interesting the SEM images of the xerogels formed by **P/18-Cu**, **P/18-2H** and **P/18-Zn** in 1,4-dioxane (Fig. 9 and Fig. S12-13) show the formation of flower-like sphere morphologies and these morphologies remain unchanged during the subsequence aging time (gels fresh prepared from 1,4-dioxane or standing over several days showing almost the same morphologies as observed by SEM, see Fig. S14). From Fig. 9 and Fig. S12-13, it can be clearly seen that the size of microsphere is not uniform and the diameter of microsphere ranges from 0.6 μm to 6.7 μm. The enlarged image of an individual sphere is presented in Fig. 9b (also in Fig. S12b, 13b and 14b), which indicates that the flower-like spheres are assembled by compact nanosheet with a thickness of ~37 nm and the whole microparticles looked like spheres. The curved nanosheet arranged either in a clockwise manner or counterclockwise manner to produce a hierarchical flow-like nano/macrostructures (Fig. 9b). The TEM images in Fig. 9b and Fig. S12b-13b shows that the flower-like spheres have a solid structure with a diameter of 1.8-5.1 μm, which are consistent with the size observed by SEM. The interaction between the solvent and the triazole units, the hydrogen bonding between the triazole units, π-π interactions, as well as van der Waals forces should play an important role in the aggregation of the compounds in solvents [26,50]. Consideration the research results of SEM, TEM and UV-vis together, the self-assembly process as well as the formation of the flower-like sphere structures can be induced as shown in Scheme S2. Since the target molecules have four triazole rings, it is easy to self-assemble in 1,4-dioxane driven by the hydrogen bonding, van der Waals and π-π interactions. By the cooperation of these intermolecular interactions, the target molecules could self-assemble into a two-dimensional (2D) nanosheet via a *J*-aggregate style which has been confirmed by UV-vis spectrum (see Table 2 and Fig. S6b). Since the molecules has four arms, these packing can principally grow in a 3D way, with large amount of molecules involved, and they finally assembled into flower-like sphere structures. So far as we know this is the first time that the spherical morphology is observed in pure porphyrin based gel system, till now only sheet-like two-dimensional or fibrous one-dimensional structures and sponge-like porous networked structures are observed in porphyrin based gel system [51,52]. The microspheres are a topic of general concern because their wide potentials as advanced functional soft materials in the fields of nonlinear optics, photo-catalysts, antibacterial materials, drug delivery, *etc*. [53,54]. Such architectures have grounded a versatile platform correlating supramolecular chemistry and soft matter science.

The organogel of **P/18-Zn** was chosen as representative to investigate its binding property towards metal ions. Copper hexahydrate perchlorate was carefully added to the top of the gel. It was observed that the dark red gel gradually collapsed from upper to bottom part and finally converted into fluid solution (Fig. S15). The collapse of gel should be resulted from the coordination between Cu^{2+} and the nitrogen atom in triazole ring, which destroyed the interaction among gelator molecules and finally destroyed the gel. Such gels with tunable and metal-ion-responsive properties, could be developed as novel functional materials.

Table 3 Gelation properties of **P/18-2H**, **P/18-Zn** and **P/18-Cu**[a]

Solvent	P/18-2H	P/18-Zn	P/18-Cu	Solvent	P/18-2H	P/18-Zn	P/18-Cu
Chloroform	S	S	S	1,4-Dioxane	G	G	G
Ethyl acetate	P	P	P	Cyclohexane	I	I	I
THF	S	S	S	Hexane	I	I	I
Methanol	I	I	I	*n*-Butanol	PG	PG	PG
Acetone	P	P	P	Toluene	P	P	P
DMF	P	P	P	DMSO	I	I	I

[a] S = solution, P = precipitation, G = gelation, PG = partial gelation, I = insoluble. Gelator concentration is 10.0 mg/mL and gel formed in an organic solvent (1-2 mL) at room temperature.

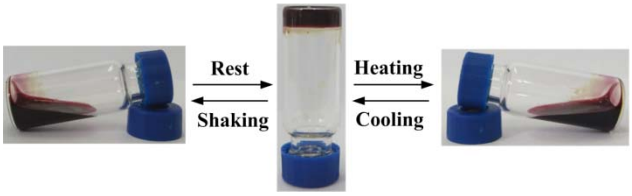

Fig. 8 Multistimuli responsive organogel of compound **P/18-2H** in 1,4-dioxane (10.0 mg/mL).

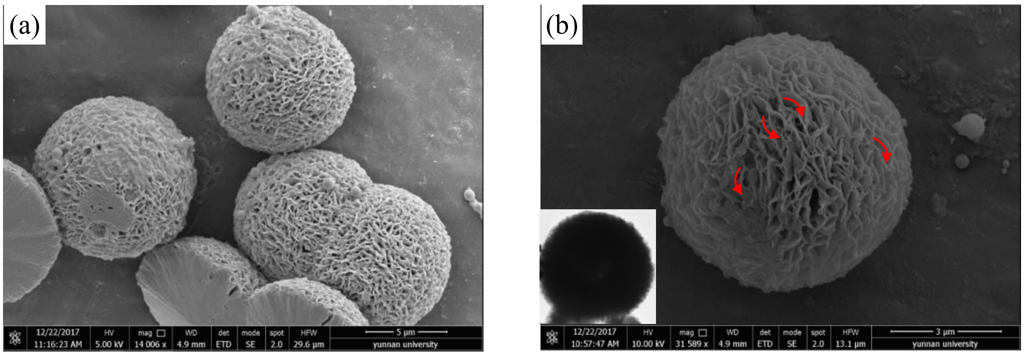

Fig. 9 SEM images of **P/18-Cu** xerogel: (a) scale bar is 5 μm; (b) scale bar is 3 μm. The inset is the TEM image, scale bar is 2 μm.

2.6 Properties of co-assembly with C_{70} or 4,7-di-4-pydriyl-2,1,3-benzothadiazole (L_1)

Porphyrin-based supramolecular complexes have attracted much attention because they can form high ordered nanostructures [55] which have potential applications in photovoltaic cells [17] and ferroelectric materials [18]. Therefore we have prepared two supramolecuar complexes: **P/18-Zn-C_{70}** and **P/18-Zn-L_1** (the preparation methods are shown in SI). The thin films of **P/18-Zn**, **P/18-Zn-C_{70}** and **P/18-Zn-L_1** have been investigated by SEM experiments (Fig. S17). The SEM image of **P/18-Zn** shows a sponge-like morphology, while that of **P/18-Zn-L_1** shows the formation of unordered layer morphology with a lot of cavities, the SEM image of **P/18-Zn-C_{70}** shows a similar sponge-like morphology like pure **P/18-Zn** but with only much fewer cavities. These microscopic studies indicated that the morphology of porphyrin **P/18-Zn** changed lot after doping with different ligands.

All these co-assembled systems display mesomorphism properties. The mesomorphic properties of these complexes were confirmed by POM (Fig. S2f-g), DSC (Fig. S3h-i) and XRD (Fig. 10a, Fig. S4f and Table S7,8).

Table 4 Transition temperatures, associated enthalpy values (in brackets) and lattice parameters of supramelcular complexes[a]

Supramolecular complex	T/°C [ΔH/kJ mol^{-1}]	a[nm] (T/°C)
P/18-Zn-C_{70}	Cr 44 [171.02] Col$_{hex}$ 130 [3.18] Iso	4.89 (110)
P/18-Zn-L_1	Cr 5 1 [189.06] Col$_{hex}$ 158 [3.02] Iso	5.29 (70)

[a] Transition temperatures were determined by DSC (10 K min^{-1}), peak temperatures from the second heating scan are given. Abbreviations: Cr = crystal; Col$_{hex}$ = hexagonal columnar phase; Iso = isotropic liquid; a = lattice parameter.

For supramolecualr complex **P/18-Zn-C_{70}**, its thermogram shows that doping with C_{70} increases the clearing temperature of compound **P/18-Zn** by 8 °C resulting in a wider mesomorphic temperature range. The SAXS pattern of **P/18-Zn-C_{70}** shows three reflections in the small angle region indexed with (10), (11) and (20) (Fig. 10a and Table S7) of a columnar hexagonal lattice (a_{hex} = 4.89 nm, T = 110 °C). This lattice parameter is almost identical with that of the columnar phase of **P/18-Zn** (a_{hex} = 4.86 nm, T = 90 °C, see Table 1). Considering the size of C_{70} (the elongated diameter is 1.1 nm) [56], the possible molecular arrangement is supposed. C_{70} is sandwiched between two porphyrin cores (Fig. 10b left) due to the strong π-donor and π-acceptor interaction [17]. The fluorescence emission of **P/18-Zn** in $CHCl_3$ was significantly quenched upon addition of C_{70} (Fig. S18), indicating the presence of electron transfer between porphyrin core and C_{70}. Additionally, uniaxial orientation of the columnar structures is readily attainable after the polydomain of the Col_{hex} phase of **P/18-Zn-C$_{70}$** is mechanically sheared within the sandwiched glass plates (Fig. S19) [57]. The macroscopically uniform alignment of columns might lead to anisotropic charge carrier transport along the molecular stacking [58]. All these properties are very important for photovoltaic (PV) applications because they can provide an efficient path for electrons or/and holes along the columnar axis, and the light-harvesting molecules are arranged with the largest area toward the coming light [17].

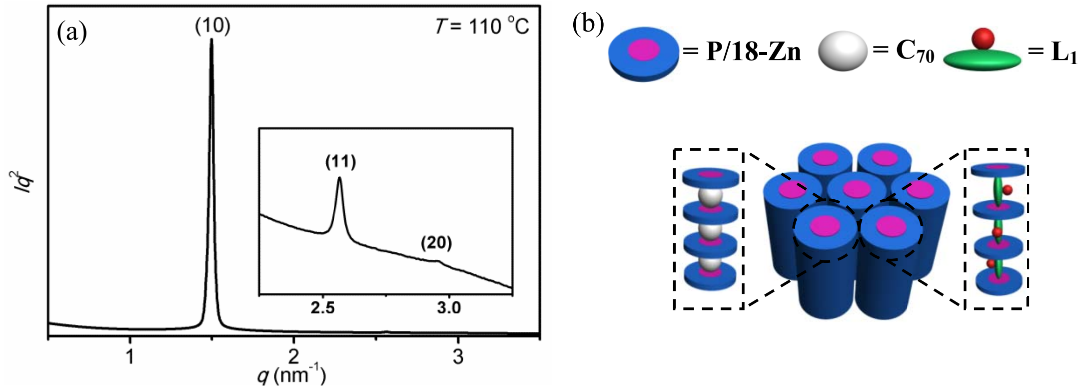

Fig. 10 (a) SAXS diffractogram of Col_{hex} phase at T = 110 °C; (b) The possible co-assembly model of Col_{hex} phase of the **P/18-Zn-C$_{70}$** (left) and the **P/18-Zn-L$_1$** (right).

For supramolecular complex **P/18-Zn-L$_1$**, the SAXS pattern shows also three reflections in the small angle region indexed with (10), (11) and (20) (Fig. S4f and Table S8) corresponding to a columnar hexagonal lattice (a_{hex} = 5.29 nm at T = 70 °C, see Table 4). This lattice parameter is a little larger than that of the columnar phase of pure **P/18-Zn** (a_{hex} = 4.86 nm at T = 90 °C, see Table 1). Considering the coordination interaction between N atom of **L$_1$** and Zinc ion of **P/18-Zn** [59], **L$_1$** should be sandwiched between two porphyrin cores (Fig. 10b right). Further, UV-vis absorption spectra show that the absorption peaks of Q band of **P/18-Zn** in solid state are at 566 nm and 608 nm (Fig. S20). Upon doping with equal molar **L$_1$**, these peaks show red shifts to 569 and 611 nm, respectively. It is accompanied by an increase in the absorption intensity. The observed red shifts and change in the intensity ratio are typical of ligand coordination in the axial position of **P/18-Zn** [18], which is in well agreement with the self-assembly model.

3 Conclusion

Collectively our simple design of self-assembling supramolecular porphyrin synthons **P/*n*-M** has enabled the construction of the hexagonal columnar LC phases as observed in the pure states of these compounds as well as in their co-assemblies with C_{70} or 4,7-di-4-pydriyl-2,1,3-benzothiadiazole, which are clearly demonstrated by POM, DSC and XRD, and the corresponding self-assembled models are well established. Further gels with unique flower-like sphere morphologies and with tunable and metal-ion-responsive properties are obtained from these compounds in 1,4-dioxane. Additionally zinc porphyrin compound **P/18-Zn** shows also selectivity exclusively for Cu^{2+} in solution. All these properties indicate that such porphyrin compounds have great potentials as self-assembled nanoscale organic electronic devices as well as chemosensors. Organic photovoltaic cells based on these porphyrin mesogens are going on.

Acknowledgements

This work was supported by National Natural Science Foundation of China (Nos. 21664015, 21364017 and 21602195) and the Yunnan Provincial Department of Education Foundation (Nos. ZD2015001, 2016FD008 and 2017FB011). We thank beamline 1W2A at Beijing Synchrotron Radiation Facility (BSRF) and beamline BL16B1 at Shanghai Synchrotron Radiation Facility (SSRF), China.

Keywords: porphyrin・liquid crystals・self-assembly・co-assembly・organogels

References

[1] a) Q. Li, *Liquid Crystals Beyond Displays: Chemistry, Physics, and Applications*, John Wiley & Sons, Hoboken, New Jersey, 2012; b) H.K. Bisoyi, Q. Li, in *Nanoscience with Liquid Crystals: From Self-Organized Nanostructures to Applications* (Ed.: Q. Li), Springer, Heidelberg, 2014, pp. 209-256.

[2] D. Adam, P. Schuhmacher, J. Simmerer, L. Häussling, K. Siemensmeyer, K.H. Etzbachi, H. Ringsdorf, D. Haarer, *Nature*. **1994**, 371, 141-143.

[3] I.O. Shklyarevskiy, P. Jonkheijm, N. Stutzmann, D. Wasserberg, H.J. Wondergem, P.C.M Christianen, A.P.H.J Schenning, Z. Tomović, J. Wu, K. Müllen, J.C. Maan, *J. Am. Chem. Soc*. **2005**, 127, 16233-16237.

[4] P. Rothemund, *J. Am. Chem. Soc*. **1936**, 58, 625-627.

[5] J.W. Goodby, P.S. Robinson, B.-K.Teo, P.E. Cladi, *Mol. Cryst. Liq. Cryst*. **1980**, 56, 303-309.

[6] J.Z. Li, H. Xin, M. Li, *Liq. Cryst*. **2006**, 33, 913-919.

[7] J.J. Miao, L. Zhu, *Chem. Mater*. **2010**, 22, 197-206.

[8] X.Y. Zhang, Y.Q. Xia, L. Zhou, P. Liu, W.J. Deng, *Tetrahedron* **2017**, 73, 558-565.

[9] J.Z. Li, T. Tang, F. Li, M. Li, *Dyes and Pigments* **2008**, 77, 395-401.

[10] S.-W. Kang, Q. Li, B.D. Chapman, R. Pindak, J.O. Cross, L.F. Li, M. Nakata, S. Kumar, *Chem. Mater*. **2007**, 19, 5657-5663.

[11] W. Liu, Y.H. Shi, T.S. Shi, G.F. Liu, Y.X. Liu, C. Wang, W.J. Zhang, *Liq. Cryst*. **2003**, 30, 1255-1257.

[12] L.F. Li, S.-W. Kang, J. Harden, Q.J. Sun, X.L. Zhou, L.M. Dai, A. Jakli, S. Kumar, Q. Li, *Liq. Cryst*. **2008**, 35, 233-239.

[13] X.L. Zhou, S.-W. Kang, S. Kang, S. Kumar, Q. Li, *Liq. Cryst*. **2009**, 36, 269-274.

[14] A. Segade, M. Castella, F. López-Calahorra, D. Velasco, *Chem. Mater*. **2005**, 17, 5366-5374.

[15] M. Castella, F. López-Calahorra, D. Velasco, H. Finkelmann, *Liq. Cryst*. **2002**, 29, 559-565.

[16] M. Castella, F. López-Calahorra, D. Velasco, H. Finkelmann, *Chem. Commun*. **2002**, 20, 2348-2349.

[17] X.L. Zhou, S.-W. Kang, S. Kumar, R.R. Kulkarni, S.Z.D. Cheng, Q. Li. *Chem. Mater*. **2008**, 20, 3551-3553.

[18] J.K.-H. Hui, H. Kishida, K. Ishiba, K. Takemasu, M.-A. Morikawa, N. Kimizuka, *Chem. Eur. J*. **2016**, 22, 14213-14218.

[19] M.A. Fazio, O.P. Lee, D.I. Schuster, *Org. Lett*. **2008**, 10, 4979-4982.

[20] K. Flavin, M.N. Chaur, L. Echegoyen, S. Giordani, *Org. Lett*. **2010**, 12, 840-843.

[21] G.D. Miguel, M. Wielopolski, D.I. Schuster, M.A. Fazio, O.P. Lee, C.K. Haley, A.L. Ortiz, L. Echegoyen, T. Clark, D.M. Guldi, *J. Am. Chem. Soc*. **2011**, 133, 13036-13054.

[22] V.S. Shetti, M. Ravikanth, *Eur. J. Org. Chem*. **2010**, 3, 494-508.

[23] O.B. Locos, C.C. Heindl, A. Corral, M.O. Senge, E.M. Scanlan, *Eur. J. Org. Chem*. **2010**, 6, 1026-1028.

[24] M. Severac, L.L. Pleux, A. Scarpaci, E. Blart, F. Odobel, *Tetrahedron Lett*. **2007**, 48, 6518-6522.

[25] T. Palacin, H.L. Khanh, B. Jousselme, P. Jegou, A. Filoramo, C. Ehli, D.M. Guldi, S. Campidelli, *J. Am. Chem. Soc*. **2009**, 131, 15394-15402.

[26] a) D. Mendoza-Espinosa, G.E. Negron-Silva, D. Angeles-Beltran, A. Alvarez-Hernandez, O.R. Suarez-Castillo, R. Santillan, *Dalton Trans*. **2014**, 43, 7069-7077; b) F. Saleem, G.K. Rao, A. Kumar, G. Mukherjee, A.K. Singh, *Organometallics* **2013**, 32, 3595-3603; c) H. Struthers, B. Spingler, T.L. Mindt, R. Schibli, *Chem. Eur. J*. **2008**, 14, 6173-6183; d) H.-F. Chow, C.-M. Lo, Y. Chen, *Top. Heterocycl. Chem*. **2012**, 28, 137-162.

[27] M. Toganoh, H. Harada, Y, Ikawa, H. Furuta, *Chem. Lett*. **2010**, 39, 252-253.

[28] X.P. Tan, L.Y. Kong, H. Dai, X.H. Cheng, F. Liu, C. Tschierske, *Chem. Eur. J*. **2013**, 19, 16303-16313.

[29] S. Cecioni, S. Faure, U. Darbost, I. Bonnamour, H. Parrot-Lopez, O. Roy, C. Taillefumier, M. Wimmerová, J.-P. Praly, A. Imbert, S. Vidal, *Chem. Eur. J*. **2011**, 17, 2146-2159.

[30] C.A Hunter, J.K.M Sanders, *J. Am. Chem. Soc*. **1990**, 112, 5525-5534.

[31] a) K. Ohta, N. Yamaguchi, I. Yamamoto, *J. Mater. Chem*. **1998**, 8, 2637-2650; b) K. Ohta, S. Azumane, W. Kawahara, N. Kobayashi, I. Yamamoto, *J. Mater. Chem*. **1999**, 9, 2313-2320; c) K. Hatsusaka, K. Ohta, I. Yamamoto, H. Shirai, *J. Mater. Chem*. **2001**, 11, 423-433; d) T. Nakai, K. Ban, K. Ohta, M. Kimura, *J. Mater. Chem*. **2002**, 12, 844-850.

[32] T. Wöhrle, I. Wurzbach, J. Kirres, A. Kostidou, N. Kapernaum, J. Litterscheidt, J.C. Haenle, P. Staffeld, A. Baro, F. Giesselmann, S. Laschat. *Chem. Rev*. **2016**, 116, 1139-1241.

[33] *CAChe 3.2*, Oxford Molecular Ltd, Oxford, UK, 1999.

[34] a) M. Prehm, F. Liu, U. Baumeister, X Zeng, G. Ungar, C. Tschierske, *Angew. Chem., Int. Ed*. **2007**, 46, 7972-7975; b) H.-J. Kim, F. Liu, J.-H. Ryu, S.-K. Kang, X. Zeng, G. Ungar, J.-K. Lee, W.-C. Zin, M. Lee, *J. Am. Chem. Soc*. **2012**, 134, 13871-13880.

[35] Another possible molecular self assembly model is shown in Fig. S5, in which the porphyrin molecule may adopt a bowl shape, *i.e.* the branched triazole wedges most likely adopt a fan shape that wrap around the stacked porphyrin core. Based on the length of the branched triazole wedges (L = 3.33 nm) and the length of the projection of the branched triazole wedges (L_{pro} = 1.51 nm) (Fig. S5), the tilt angle θ of approximately 63° with respect to the cross section of the column was estimated. Related hexagonal columnar phase was form by bowl shaped petidic macrocycles: K. Sato, Y. Itoh, T. Aida. *J. Am. Chem. Soc.* **2011**, 133, 13767-13769.

[36] M. Nappa, J.S. Valentine, *J. Am. Chem. Soc*. **1978**, 100, 5075-5080.

[37] C. Tekuri, D.K. Singh, M. Nath, *Dyes and Pigments* **2016**, 132, 194-203.

[38] T. Kishida, N. Fujita, K. Sada, S. Shinkai, *Langmuir* **2005**, 21, 9432-9439.

[39] M. Hamaguchi, H. Sawada, J. Kyokane, K. Yoshino, *Chem. Lett*. **1996**, 7, 527-528.

[40] K.L. Cunningham, K.M. McNett, R.A. Pierce, K.A. Davis, H.H. Harris, D.M. Falck, D.R. McMillin, *Inorg. Chem*. **1997**, 36, 608-613.

[41] X.P. He, Z. Song, Z.Z. Wang, X.X. Shi, K. Chen, G.R. Chen, *Tetrahedron* **2011**, 67, 3343-3347.

[42] S. Cao, Z. Pei, Y. Xu, R. Zhang, Y. Pei, *RSC Adv.* **2015**, 5, 45888-45896.

[43] D.-H. Xie, X.-J. Wang, C. Sun, J. Han, *Tetrahedron Lett.* **2016**, 57, 5834-5836.

[44] D.T. Shi, B. Zhang, Y.X. Yang, C.-C. Guan, X.-P. He, Y.-C. Li, G.-R. Chen, K.X. Chen, *Analyst* **2013**, 138, 2808-2811.

[45] R. Krämer, *Angew. Chem. Int. Ed*. **1998**, 37, 772-773.

[46] A. Friggeri, B. L. Feringa, J. van Esch, *J. Controlled Release* **2004**, 97, 241-248.

---

[47] V. K. Praveen, S. J. George, R. Varghese, C. Vijayakumar, A. Ajayaghosh, *J. Am. Chem. Soc*. **2006**, 128, 7542-7550.

[48] R. M. Yang, S. H. Peng, T. C. Hughes, *Soft Matter* **2014**, 10, 2188-2196.

[49] a) K. Murata, M. Aoki, T. Suzuki, T. Harada, H. Kawabata, T. Komori, F. Ohseto, K. Ueda, S. Shinkai, *J. Am. Chem. Soc.* **1994**, 116, 6664-6676; b) K. Yoza, N. Amanokura, Y. Ono, T. Akao, H. Shinmori, M. Takeuchi, S. Shinkai, D.N. Reinhoudt, *Chem. Eur. J.* **1999**, 5, 2722-2729.

[50] a) B.P. Krishnan, K.M. Sureshan, *J. Am. Chem. Soc*. **2017**, 139, 1584-1589; b) R. Balamurugan, Y.-S. Zhang, S. Fitriyani, J.-H. Liu, *Soft Matter* **2016**, 12, 5214-5223.

[51] T. Kishida, N. Fujita, K. Sada, S. Shinkai, *Langmuir* **2005**, 21, 9432-9439.

[52] L. Zeng, P. Liao, H. Liu, L. Liu, Z. Liang, J. Zhang, L. Chen, C.Y. Su, *J. Mater. Chem. A*. **2016**, 4, 8328-8336.

[53] a) S.S. Babu, H. Möhwald, T. Nakanishi, *Chem. Soc. Rev*. **2010**, 39, 4021-4035; b) C.J. Medforth, Z. Wang, K.E. Martin, Y. Song, J.L. Jacobsen, J.A. Shelnutt, *Chem. Commun*. **2009**, 7261-7277; c) Y. Li, T. Liu, H. Liu, M.-Z. Tian, Y. Li, *Acc. Chem. Res*. **2014**, 47, 1186-1198; d) H. Liu, J. Xu, Y. Li, Y. Li, *Acc. Chem. Res*. **2010**, 43, 1496-1508; e) T. Hasobe, *J. Phys. Chem. Lett*. **2013**,4, 1771-1780; f) K. Ariga, T. Nakanishi, J.P. Hill, *Curr. Opin. Colloid Interface Sci*. **2007**, 12, 106-120; g) J. Pecher, S. Mecking, *Chem. Rev*. **2010**, 110, 6260-6279.

[54] X. Zhang, Y.P. Wang, P.L. Chen, P.P. Guo, M.H. Liu, *RSC Adv*. **2015**, 5, 78427-78435.

[55] a) C.M. Xue, O. Birel, Y.N. Li, X. Ma, M. Gao, A. Urbas, Q. Li, *J. Colloid Interface Sci.* **2013**, 398, 1-6; b) C.M. Xue, Y.Q. Xu, Y. Pang, D.S. Yu, L.M. Dai, M. Gao, A. Urbas, Q. Li, *Langmuir* **2012**, 28, 5956-5963.

[56] L.P. Hernández-Eguía, E.C. Escudero-Adán, I.C. Pintre, B. Ventura, L. Flamigni, P. Ballester, *Chem. Eur. J.* **2011**, 17, 14564-14577.

[57] a) M. Yoshio, T. Mukai, H. Ohno, T. Kato, *J. Am. Chem. Soc*. **2004**, 126, 994-995; b) M. Yoshio, T. Kagata, K. Hoshino, T. Mukai, H. Ohno, T. Kato, *J. Am. Chem. Soc*. **2006**, 128, 5570-5577.

[58] a) I.O. Shklyarevskiy, P. Jonkheijm, N. Stutzmann, D. Wasserberg, H.J. Wondergem, P.C.M. Christianen, A.P.H.J. Schenning, D.M.D. Leeuw, Ž. Tomović, J. Wu, K. Müllen, J.C. Maan, *J. Am. Chem. Soc*. **2005**, 127, 16233-16237; b) A.M. van de Craats, N. Stutzmann, O. Bunk, M.M. Nielsen, M. Watson, K. Müllen, H.D. Chanzy, H. Sirringhaus, R.H. Friend, *Adv. Mater*. **2003**, 15, 495-499.

[59] J.K.-H. Hui, H. Kishida, K. Ishiba, K. Takemasu, M.-A. Morikawa, N. Kimizuka, *Chem. Eur. J*. **2016**, 22, 14213-14218.